Quantum information processing with trapped electrons and superconducting electronics

2013 New J. Phys. 15 073017

(http://iopscience.iop.org/1367-2630/15/7/073017)

New Journal of Physics
The open access journal for physics

Quantum information processing with trapped electrons and superconducting electronics

Nikos Daniilidis[1,4], Dylan J Gorman[1], Lin Tian[2] and Hartmut Häffner[1,3]

[1] Department of Physics, University of California Berkeley, Berkeley, CA 94720, USA
[2] School of Natural Sciences, University of California Merced, Merced, CA 95343, USA
[3] Materials Sciences Division, Lawrence Berkeley National Laboratory, Berkeley, CA 94720, USA
E-mail: nikos.daniilidis@gmail.com

New Journal of Physics **15** (2013) 073017 (19pp)
Received 17 April 2013
Published 5 July 2013
Online at http://www.njp.org/
doi:10.1088/1367-2630/15/7/073017

Abstract. We describe a parametric frequency conversion scheme for trapped charged particles, which enables a coherent interface between atomic and solid-state quantum systems. The scheme uses geometric nonlinearities of the potential of coupling electrodes near a trapped particle, and can be implemented using standard charged-particle traps. Our scheme does not rely on actively driven solid-state devices, and is hence largely immune to noise in such devices. We present a toolbox which can be used to build electron-based quantum information processing platforms, as well as quantum hybrid platforms using trapped electrons and superconducting electronics.

[4] Author to whom any correspondence should be addressed.

Contents

1. Introduction

The experimental realization of an operational quantum computer is a well defined problem [1], but after nearly two decades of intense experimental pursuit, the choice of the optimal physical system remains a difficult task [2]. Solid-state based systems offer fast gate operation times and straightforward fabrication scalability, while atomic systems show remarkable coherence times [2, 3]. It appears appealing to bridge the gap between atomic and solid-state based quantum devices, and combine them into quantum hybrid systems that exploit the benefits of both approaches. Such hybrids can combine the speed of the former with the long coherence times of the latter. Moreover, such platforms can interconnect atomic qubits via a solid-state quantum bus [4], and thus address the scalability challenges of atomic qubits. Finally, quantum state initialization and read-out can be based on such hybrid interfaces. This is an essential feature for atomic systems where these tasks are not straightforward, such as trapped-electron based quantum information processing (QIP) [5]. A successful interface will allow sufficient control over the long-lived internal state of the atomic system, such that we can initialize it in an arbitrary quantum state, swap it with a quantum state in the circuit and read it out with high fidelity.

In many cases, the atomic and solid-state qubits couple weakly to each other, and it is beneficial to interconnect them via intermediate systems, acting as buses for quantum information [6, 7]. A versatile solution is to use harmonic oscillators as buses, whose properties can be tailored to specific applications. In this respect, electrical oscillators are useful for the solid-state side, while trapped-particle motion offers benefits as a bus on the atomic side [7].

The motional state of charged particles, for example ions trapped in radio frequency (Paul) traps or electrons in Penning traps, couples to electrical oscillators [8] and thus the problem of building a hybrid quantum interface relies on understanding and overcoming the constrains imposed by the electrical and motional oscillators.

Single ions can be trapped with very long storage times, their motional and electronic quantum state can be controlled to a very high degree, and the motional state can be mapped onto a long-lived electronic or spin state of the ion using standard techniques [3]. A major challenge lies in the frequency mismatch between the ion motion, typically 1–10 MHz, and the superconducting circuits, with transitions between 4 and 10 GHz. The frequency gap can be bridged with parametric frequency conversion [8]. One possibility is to actively drive some circuit element, for example as proposed by Kielpinski *et al* [9] in a scheme suitable for upconversion from 1 MHz to 1 GHz. An additional challenge for such frequency conversion schemes is that the small charge induced by the ion motion, of order 10^{-4} elementary charges, needs to overcome low-frequency noise in the solid state. Thus, there is need of a frequency conversion mechanism which upconverts the trapped particle frequency to the microwave range *before* this enters the solid state, since such a scheme would be naturally immune to $1/f$ noise in the solid state.

Electrons offer a number of benefits compared to ions, due to their large charge-to-mass ratio. Most importantly, their motional state has a large electric dipole moment which can couple strongly to electrical circuits [10, 11]. Electrons can be trapped with high motional frequencies and long storage times, using oscillating trapping potentials in the microwave range [12, 13], or in Penning traps. The frequencies of non-magnetically trapped electrons could reach the microwave regime while operating the electron traps with realistic voltages, provided the trapping structures are made sufficiently small, 1μm or smaller. Nevertheless, such miniaturized traps for electrons are likely to face limitations due to poorly understood electric field noise arising from nearby surfaces [14, 15]. Thus, alternative solutions which will work for electrons trapped in larger trap structures, in the several micrometer range, are needed. Pennning traps offer one such possibility [16], but complications arise due to the presence of strong magnetic fields if the electrons are trapped in a Penning trap. Thus a frequency conversion scheme for electrons trapped in the low magnetic environment of an RF trap would have significant advantages over the above-mentioned approaches.

Here we describe a parametric frequency conversion scheme which uses the quadrupolar potential of a trap electrode in combination with classically driven particle motion in order to couple the motional degree of freedom of a trapped particle to electrical resonators. This scheme uses the trapping structure itself to achieve the frequency conversion, i.e. it does not require additional, actively driven elements. Moreover, it upconverts the motional signal of any charged trapped particle before it enters the solid-state circuit, and thus reduces the impact of $1/f$ noise, which is present in typical solid-state devices. We show how, using this scheme, one can swap and entangle the motion of a single electron with a transmon qubit. We also describe how to use our scheme to cool the motion of a single electron to the ground state, and to couple electrons in separate traps. Based on these tools, we describe hybrid QIP platforms which are based on single electrons in Paul traps and superconducting microwave electronics. We also discuss the possibility of using this scheme to parametrically couple electrons to circuit elements at higher frequencies, above 100 GHz.

The paper is organized as follows. In section 2 we discuss the parametric coupling mechanism, and in section 3 we describe the physical components needed to implement

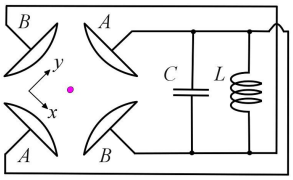

Figure 1. Basic setup for parametric frequency conversion. A particle (shown in magenta) is trapped in a harmonic potential, between electrodes which create a strong quadrupole potential around the trapping position. The electrodes are connected to a resonant circuit, allowing the particle motion to couple to the modes of the circuit.

this mechanism using a ring Paul trap for trapped electrons. We then describe some basic applications of this scheme and outline the main decoherence sources which are expected to limit basic operation fidelities. The applications we describe form a toolbox which can be used to build several interesting devices such as: a QIP platform with electron–spin memory and Josephson junction (JJ) processing qubits, and two variants of an all-electron QIP platform, with JJ qubits used for the electron state readout.

2. Parametric coupling mechanism

A mechanism allowing to coherently swap the motion of a single trapped electron with the field of a microwave resonator, opens up the possibility of coupling the electron to any type of superconducting qubit which can be coupled to the microwave resonator. We now describe such a coupling mechanism for electrons and microwave resonators.

In order to couple the motion of a trapped particle to a microwave resonator, the problem of the frequency gap between the particle motion and the circuit resonance needs to be solved. When a particle is trapped between electrodes which create a spatially nonlinear potential, the force on the particle in response to voltages applied to the electrodes depends on the particle position, in other words the coupling strength between the particle and a circuit connected to the electrodes depends on the position. This implies that if we drive the particle position at an appropriate frequency, then the coupling strength is modulated at the difference frequency between the particle and the circuit resonance, and thus we can couple the two. Here we consider this mechanism in trapping structures with a quadratic nonlinearity, i.e. electrodes with a quadrupolar potential. The pump for this parametric coupling process is a classical voltage which drives the particle motion.

We consider a charged particle trapped in a harmonic potential. The particle is located between two sets of coupling electrodes which are connected to an electrical resonator, as in figure 1. The circuit couples to the position of a particle in the trap via the voltage on the coupling electrodes. The interaction energy is $qU(\mathbf{r})V$, where q is the charge and $\mathbf{r}$ the position of the particle, V is the voltage between the coupling electrodes and $U(\mathbf{r})$ the potential at position $\mathbf{r}$, when 1 V is applied to the coupling electrode. For simplicity, here we consider coupling electrodes which create electric quadrupoles of the form $\sum_{i=x,y,z} s_i(r_i/D_{2,i})^2$, $s_i = \pm 1$, but the analysis can be generalized to potentials containing cross terms as well. For a displacement in the direction r_i, $i = x, y, z$, around the trapping position, the potential can

be expanded as $U(r_i) = U(0) + (r_i/D_{1,i}) + s_i(r_i/D_{2,i})^2 + O(r^3)$.[5] Then, the Hamiltonian for the trapped particle and the circuit is, to second order in r_i

$$H = H_{\text{circuit}} + H_{\text{motion}} + \sum_i \frac{q\,Q}{C}\left(\frac{r_i}{D_{1,i}} + s_i\frac{r_i^2}{D_{2,i}^2}\right), \tag{1}$$

where $H_{\text{circuit}} = \frac{Q^2}{2C} + \frac{\Phi^2}{2L}$, $H_{\text{motion}} = \sum_i \frac{p_i^2}{2m} + \frac{m\omega^2 r_i^2}{2}$ are the Hamiltonians describing the circuit and the particle motion. Here, r_i is the particle displacement and $p_i = m\dot{r}_i$ the particle canonical momentum. C is the effective capacitance of the resonator and Φ the flux variable at the coupling electrode. Also $Q = C\dot{\Phi} - q\,U(r_i) + Q_{\text{d}}(t)$ is the canonically conjugate charge, which includes the charge, $qU(r_i)$, induced on the electrode by the moving particle, and a classical, time-dependent charge $Q_{\text{d}}(t)$, induced from the classical parametric drive voltage. The latter can interfere with coherent quantum operations, but, as we discuss in appendix A, it is detuned by the trap frequency, ω_i, from all resonant modes in the system and can be made negligibly small by carefully balancing the different electrode capacitances in the device.

The coupling term linear in position, $q\,Q\,r_i/(C\,D_{1,i})$, couples the circuit and the particle when the two are resonant, and the quadratic terms, $q\,Q\,r_i^2/(C\,D_{2,i}^2)$, lead to parametric coupling. To switch on the parametric action, we drive classical particle motion, $r_{\text{d},i} = A_{\text{d}}\cos(\Omega_{\text{d}}t)$, in addition to the quantum motion in the trapping potential, $\hat{r}_i$. We decompose the particle position as $r_i = r_{\text{d},i} + \hat{r}_i$. Expanding the quadrupole part of the interaction energy, we obtain the parametric coupling term $\frac{2q\,\hat{Q}\,r_{\text{d}}\,\hat{r}_i}{C\,D_{2,i}^2} = \frac{2q\,A_{\text{d}}}{C\,D_{2,i}^2}\cos(\Omega_{\text{d}}t)\hat{Q}\hat{r}_i$, where $\hat{Q}$ is the quantum charge degree of freedom in the circuit. When driving motion in the y-direction, the Hamiltonian in the interaction picture now becomes

$$H_{\text{er}} = \hbar g\cos(\Omega_{\text{d}}t)(\mathrm{e}^{\mathrm{i}(\Omega-\omega_y)t}a_\phi^\dagger a_y + \mathrm{e}^{\mathrm{i}(\Omega+\omega_y)t}a_\phi^\dagger a_y^\dagger + \text{h.c.}). \tag{2}$$

The a_ϕ, and a_y operators correspond to the circuit and particle modes respectively. $\Omega = 1/\sqrt{LC}$ is the circuit resonant frequency, ω_y the particle frequency and $\hbar g = \frac{2\,q\,V_0\,A_{\text{d}}\,y_0}{D_{2,y}^2}$. $y_0 = \sqrt{\hbar/(2\,m\omega_y)}$ describes quantum fluctuations of the particle position, and $V_0 = \Omega\sqrt{\hbar\,Z/2}$ quantum fluctuations of the circuit charge variable, which depends on the characteristic impedance $Z = \sqrt{L/C}$.

If $\Omega_{\text{d}} = \Omega - \omega_y$, then the terms $(\mathrm{i}\,a_\phi^\dagger a_y + \text{h.c.})$ of equation (2) survive in the rotating wave approximation. The system operates as a parametric frequency converter, with the classical drive providing pump photons which allow coherent coupling between the particle and the resonator. Population exchange between the two modes occurs with a parametric coupling rate $g_{\text{p}} = g/2$ [17]. If $\Omega_{\text{d}} = \Omega + \omega_y$, then the system behaves as a parametric amplifier [17]. The effective Hamiltonian then has the form $(\mathrm{i}\,a_\phi^\dagger a_y^\dagger + \text{h.c.})$ which generates two-mode squeezing of the coupled modes [18]. Provided a sufficiently low-noise classical drive, parametric frequency conversion can couple two non-resonant systems with no added noise [19]. The fidelity of coupling between charged particles and electrical circuits will be limited by motional decoherence of the particle motion, decoherence in the resonator and superconducting qubit circuits, and classical noise in the trap drive and the parametric drive.

In what follows, we focus on using this mechanism as a frequency converter. We also focus on electrons, which due to their large charge-to-mass ratio can couple strongly to microwave

[5] At the trapping position, the terms of odd order can be made vanishingly small by symmetry, and the higher than quadratic terms in r_i can be made negligibly small.

circuits using currently attainable experimental parameters. In section 4 we discuss applications of this scheme: i.e. quantum state initialization for the electron, creation of entanglement and quantum state transfer between single electrons and superconducting qubits, as well as creation of entanglement and quantum state transfer between distant electrons.

3. Physical systems

As already mentioned, the central application we aim at, is the coherent coupling of trapped electrons to superconducting qubits. To minimize the effects of decoherence, we choose to couple electrons to the superconducting qubit which currently exhibits the longest coherence times, namely the 'three-dimensional' (3D) transmon qubit [20, 21]. The transmon is a 'Cooper pair box' qubit in which the JJ capacitance is increased to make the device largely immune to charge noise [22], and operation of this qubit inside a 3D microwave cavity further suppresses decoherence in this device [20]. Here we assume this implementation of superconducting qubits, and assume decoherence times $\tau_1 = 70\,\mu$s and $\tau_2 = 92\,\mu$s, as those in [21].

For simplicity, we choose here a ring trap to trap single electrons (figure 2). This kind of trap combines high trap depth, low anharmonicity of the trapping potential, and strong parametric coupling. We simulated this design with $D = 30\,\mu$m, $R_0 = 5\,\mu$m, $\alpha = 20^\circ$ (see figure 2 for an explanation of the parameters) using an electrostatics solver [23]. The effective coupling length appearing in equation (1) is $D_{2,y} \approx 15\,\mu$m. Single electrons with secular frequencies $\omega_y = 2\pi \times 500\,$MHz, $\omega_{x,z} \approx 2\pi \times 400\,$MHz, can be trapped with trap depth of 1 meV using a trap drive on the central ring electrode (shown in yellow) at $\Omega_{\rm tr} \approx 2\pi \times 7\,$GHz, amplitude of approximately 0.4 V, and with a static bias of a few hundred mV on the trap electrodes. In what follows, we assume a heating rate of 8100 motional quanta s^{-1} for the electron motion (i.e. $\tau_1 \approx 123\,\mu$s). We estimate this heating rate by assuming that the electric field noise measured with ions in cryogenic traps is caused by noise sources on the electrode surfaces [15], and by rescaling the measured values of ion trap noise [24] as appropriate for the geometry and frequency of the electron trap (see appendix B).

To implement the parametric coupling scheme, we can drive electron motion in the y-direction at $\Omega_{\rm d} = \Omega_{\rm tr}$ and $A_{\rm d} = 750\,$nm, by applying opposite oscillating voltages of amplitude 0.4 V on the top and bottom ring electrodes (orange). Numerical integration of the equations of motion shows that the trap is stable under this condition (see appendix C). The trapping potential and the parametric pump drive will not significantly limit the fidelities of processes described in section 4, if they are stable to better than 1 part in 10^3. The capacitances between the tip electrodes and the ring electrodes in this structure range from 0.3 to 0.8 fF. While this will have only a small loading influence on the resonator to which the particle motion will couple, the resonator can be off-resonantly excited by the parametric drive and the trapping potential. We discuss solutions to these technical issues in appendix A.

To load single electrons in the ring trap, one option is to have the trap fabricated at the end of a linear Paul trap with segmented electrodes [25]. The linear trap can have a taper from large trap dimensions to smaller dimensions [26] to load electrons at high energy and resistively cool them [10] in different stages (e.g. precooling to 10 K, followed by cooling to 1 K to load into the ring trap). Electron clouds can be loaded in the linear trap using a heated filament, or, in order to have better control on the number of created electrons, by photoionization of an atomic vapor. After the electron cloud is cooled to 1 K, the number of electrons in the trap can be distinguished by coupling their motion to an electrical resonator at the electron resonance

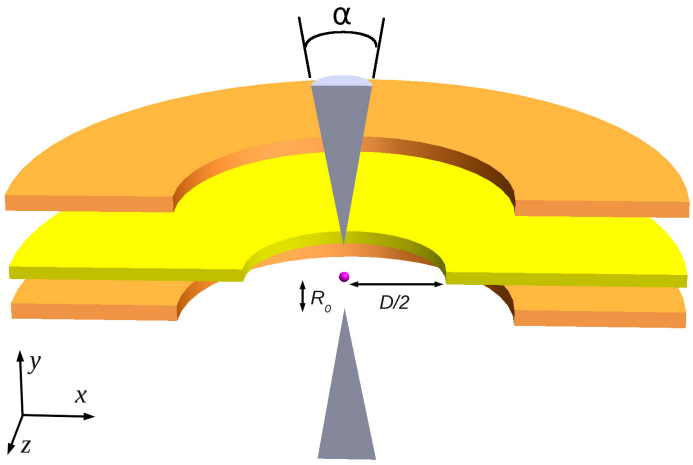

Figure 2. A ring trap with two sharp tip electrodes (trapped electron in magenta). The trapping ponderomotive pseudopotential is created by a ring electrode (yellow) with inner diameter D. Two conical tip electrodes (gray) with opening angle α are located a distance R_0 from the trapping position in the y-direction. These can be connected to an external circuit, allowing to couple the particle motion to the circuit. Two ring electrodes (orange) can classically drive the particle motion. With this configuration, the gray electrodes correspond to the electrodes labeled 'A' in figure 1, while the yellow and orange correspond to 'B'. To achieve parametric coupling, we drive electron motion in the y-direction with amplitude A_d, but driving motion in the xz-plane is also possible. An equivalent alternative configuration for trapping and parametric coupling, is to connect the middle ring electrode (yellow) to an electrical resonator, connect the top and bottom tip electrodes (gray) to the source of the trapping ponderomotive potential, and use the top and bottom ring electrodes (orange) for the parametric drive.

frequency [10], and the segmented trap electrodes can be used to heat and split the electron cloud until a single electron is trapped [27]. Finally, the electron can be transported into the ring trap, and 'locked' in place by modifying the ponderomotive trapping potentials of the linear trap and the segmented trap [28, 29].

The resonator depicted schematically in figure 1 can be a lumped-element resonator, or a coplanar waveguide (CPW) resonator. The coupling strength between an electrical resonator and the particle in the trap will benefit from high characteristic impedance resonators, due to the $\sqrt{Z}$ dependence of quantum voltage fluctuations on the characteristic impedance Z. The effective impedance Z for a CPW section with length $n\lambda/4$, $n = 1, 2, \ldots$ is related to the CPW characteristic impedance, Z_CPW, by $Z = \frac{4\,Z_\mathrm{CPW}}{n\,\pi}$. In what follows, we consider a resonator with characteristic impedance 1 kΩ. TiN-based high kinetic inductance resonators [32] are promising in this respect. Using this technology, resonators with high inductance per unit length, exceeding $\approx$60 pH μm^{-1}, have been achieved [33]. Designing resonators based on such films, with gap between the center conductor and the ground plane in the tens of μm range would achieve the required impedance of approximately 1 kΩ. In what follows, we assume a resonator with quality factor similar to the best value obtained by Megrant *et al* [30] with $\tau_1 = 45\ \mu$s at $\approx 2\pi \times 7$ GHz (see appendix D).

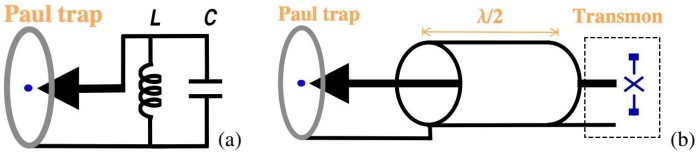

Figure 3. Circuits for electron–resonator and electron–transmon coupling. (a) An electron in a ring trap, with the tip electrodes connected to a microwave LC resonator with impedance $Z = \sqrt{L/C}$. (b) Schematic drawing of an electron coupled via a $\lambda/2$ section of a coplanar transmission line to a transmon in a cavity [20]. For superconducting coplanar resonators in the GHz range, internal quality factors of more than 10^6, corresponding to damping times of $\approx 45\,\mu$s, have been achieved [30]. To achieve high characteristic impedance, $Z = 1\,\mathrm{k}\Omega$, and internal quality factors $Q > 10^6$, high kinetic inductance resonators based on thin TiN films can be used [31].

4. Applications

4.1. Electron–resonator coupling

In order to couple the electron to a microwave circuit, we consider the tip electrodes to be connected to the open end of a $\lambda/4$ superconducting CPW resonator, or a lumped element resonator (figure 3(a)). In the case of a CPW, quantization of the resonator mode can be treated as in [34]. With trap frequency $\omega_y = 2\,\pi \times 500\,\mathrm{MHz}$, driven motion $A_\mathrm{d} = 750\,\mathrm{nm}$, $\Omega = 2\pi \times 7\,\mathrm{GHz}$ and $Z = 1\,\mathrm{k}\Omega$, the coupling rate is $g_\mathrm{p} = 2\,\pi \times 1.1\,\mathrm{MHz}$. This allows complete population exchange between the motion of a single electron and a $2\pi \times 7\,\mathrm{GHz}$ resonator in $\tau_\mathrm{swap} \approx 230\,\mathrm{ns}$. By turning on the parametric coupling between an electron resistively precooled to $\sim$1 K [8] and a microwave resonator at 30 mK, for time τ_swap, the electron motion can be prepared to its ground state with approximately 99.8% fidelity. The fidelity of this operation is limited by the heating of the electron motion during the swap operation (see section 3), and can serve as a quantum-state initialization step in the context of QIP.

4.2. Electron–transmon coupling

For a specific example of a hybrid quantum device realizable under our scheme, we consider the case of coupling an electron to a transmon through an intermediary transmission line, as shown schematically in figure 3. The tips of the Paul trap are connected to the open end of a $\lambda/2$ CPW resonator, which couples the y electron oscillation to the resonator. The transmon is operated inside a 3D cavity, an architecture which provides increased coherence times [20]. The second open end of the $\lambda/2$ resonator extends into the cavity, allowing it to couple to the TE_{011} mode of the cavity with a rate $G_\mathrm{lc} \approx 2\,\pi \times 3\,\mathrm{MHz}$ (appendix E). The transmon is very strongly coupled to the cavity, with coupling constant G_tc in the $2\pi \times 100\,\mathrm{MHz}$ regime [20]. The cavity–transmon detuning satisfies $\Delta = \Omega_\mathrm{c} - \Omega_\mathrm{t} \gg G_\mathrm{tc}$, i.e. the system is operated in the dispersive regime and the state that the resonator couples to is a dressed transmon state with transition frequency ω_t. Adiabatically eliminating the cavity, yields an effective coupling rate $G_\mathrm{lt} = G_\mathrm{lc}G_\mathrm{tc}/\Delta$ between the transmission line and the dressed transmon (appendix F). The effective Hamiltonian for the

electron–resonator–transmon system is

$$H_{\rm et} = H_{\rm er} + \hbar g_{\rm p}(e^{-i\delta t} a_\phi^\dagger \sigma^- + {\rm h.c.}), \tag{3}$$

where σ^- is the Pauli spin lowering operator for the transmon qubit, we have allowed for a detuning $\delta = \Omega_{\rm r} - \omega_{\rm t}$ between the resonator and the transmon, and we choose a parametric drive $\Omega_{\rm d} = \omega_{\rm t} - \omega_y - \delta$ in $H_{\rm er}$ (equation (2)). To optimize state transfer we choose Δ such that $G_{\rm lt} = g_{\rm p}$.

The detuning δ is necessary to produce maximally entangled states of the electron motion and the transmon (i.e. Bell states), and reduces the decoherence induced by losses in the bus. For an arbitrary detuning, this Hamiltonian will not generate complete state transfer between the electron and the transmon, because some population will, in general, be left in the transmission line. However, by choosing a 'magic' detuning $\delta_n = \sqrt{\frac{8n^2}{2n+1}} g_{\rm p}$, $n = 1, 2, \ldots$ full state exchange will occur between the electron and the transmon in $\tau_{\rm swap} = \frac{\pi}{g_{\rm p}} \sqrt{\frac{2n+1}{2}}$, and the two are in a Bell state at $\tau_{\rm swap}/2$. This situation is similar to the Mølmer–Sørensen gate for trapped ions [35]. Using the parameters quoted above for the electron traps and for the microwave resonator, electron–transmon state transfer is achieved in 560 ns. By numerically solving the Lindblad master equation of the coupled system (see figure 4), we find a fidelity for state exchange of 98.8% for the $n = 1$ magic detuning. At time $\tau_{\rm swap}/2 \approx 280$ ns the electron and the transmon are in the Bell state $\frac{1}{\sqrt{2}}(|0, 1\rangle - i\,|1, 0\rangle)$ with fidelity 99.4%. With our set of parameters, these fidelities are limited mainly by losses in the resonator and by heating of the electron motion (see section 3). For the $n = 0$ magic detuning, an electron–transmon swap operation is completed in 320 ns with fidelity 99.4%.[6]

4.3. Electron–electron coupling

An additional application of this parametric scheme is in coupling electrons in separate traps via a microwave bus. If both ends of the $\lambda/2$ CPW are connected to the coupling tips of two electron traps, the electron in each trap gets coupled to the microwave bus with parametric coupling constant $g_{\rm p}$. Using the same 'magic' detuning idea as above and the parameters of figure 4, we find that the two motional states can be entangled with each other within $\tau_{\rm swap}/2 \approx 280$ ns with fidelity 99.2%, and swapped within $\tau_{\rm swap} \approx 560$ ns, with fidelity 98.3%. For the $n = 0$ magic detuning, an electron–electron swap operation is completed in 320 ns with fidelity 99.1%.

4.4. Spin–motion coupling

In order to take full advantage of the low decoherence of the trapped electron system, we now consider mapping the electron motional state to its spin. We can define an electron spin manifold with splitting in the radio-frequency range, e.g. $\omega_{\rm s} = 2\pi \times 28$ MHz using a static bias field of 10^{-3} T, see figure 5(a). To map the motional state on the spin and vice versa, we consider a coupling mechanism implemented already with trapped ions [36, 37]. Microfabricated coils near the trap generate an oscillating magnetic field with frequency $\omega_y - \omega_{\rm s}$, thus driving a transition between the electron motion and its spin. Using a Helmholtz coil geometry with

[6] An additional possibility is to perform the swap operations by adiabatically changing the electron–resonator and resonator–transmon coupling strengths. Such schemes will be significantly slower than the one we describe here (requiring $\tau_{\rm swap} \gg 1/g_{\rm p}$), and will thus suffer more from decoherence sources.

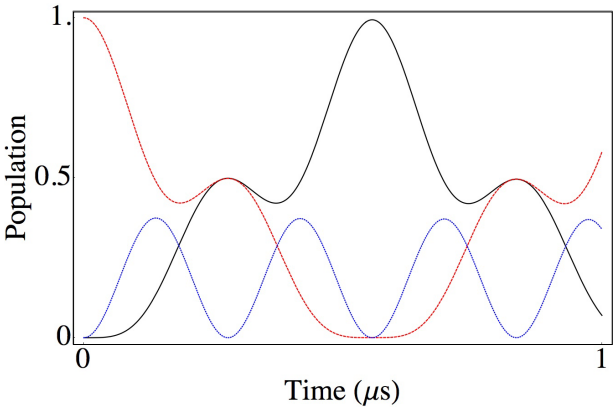

Figure 4. Populations derived from a numerical solution of the Lindblad master equation for the electron motional mode ($\langle a_y^\dagger a_y \rangle$, red), the transmission line ($\langle a_\phi^\dagger a_\phi \rangle$, blue) and the dressed transmon ($\langle \sigma_z \rangle$, black), for the $n = 1$ magic detuning (see text). The parametric coupling rate is $g_\mathrm{p} = 2\pi \times 1.1$ MHz. The initial state is $|1, 0, 0\rangle$, and the fidelity of evolution to the state $|0, 0, 1\rangle$ after $\tau_\mathrm{swap} \approx 560$ ns is 98.8%. At $\tau_\mathrm{swap}/2$, the electron and the transmon are entangled in the state $|1, 0\rangle - \mathrm{i}\,|0, 1\rangle$, with fidelity 99.4%. For the $n = 0$ detuning, an electron–transmon swap operation is completed in 320 ns with fidelity 99.4%, and an electron–electron swap with fidelity 99.1%. For these simulations, we assumed the electron heating rate to be 8100 motional quanta s^{-1} ($\tau_1 \approx 123\,\mu$s), the transmon decoherence times $\tau_1 = 70\,\mu$s, $\tau_2 = 92\,\mu$s [21], and the resonator damping time $\tau_1 = 45\,\mu$s [30] (see section 3).

radius 50 μm, driven such that only a quadrupole magnetic field is generated at the electron, an oscillating current of 1 A, and frequency of 472 MHz can drive spin–motion transitions with Rabi frequency $2\pi \times 410$ kHz. Here, we assumed again $\omega_y = 2\pi \times 500$ MHz, and $\omega_\mathrm{s} = 2\pi \times 28$ MHz, corresponding to a static bias field of 10^{-3} T. The electron motional state can be mapped onto the spin in approximately 610 ns, with 99.5% fidelity. The coils which generate the oscillating magnetic fields can be thermally anchored on a 1 K refrigeration stage to minimize heat load on the 30 mK stage, which is necessary for the superconducting electronics.

In order to preserve the phase coherence of the electron spin, the magnetic field at the electron needs to be stabilized. By stabilizing the magnetic field to $14\,\mathrm{pT}/\sqrt{\mathrm{Hz}}$, the coherence time of the electron spin will exceed 1 s. This noise requirement is three orders of magnitude less stringent than those achieved with magnetic field shielding in superconducting quantum interference device (SQUID) magnetometery [38]. Heating of the electron motion in a spatially inhomogeneous magnetic field will cause additional dephasing. This can be mitigated by engineering a homogeneous static magnetic field, and by periodically cooling the electron motion to its ground state.

5. Outlook

The elementary toolbox described in section 4 can be used in hybrid QIP platforms in which the electron spin serves as a quantum memory, and the electron motion as a bus for coupling to

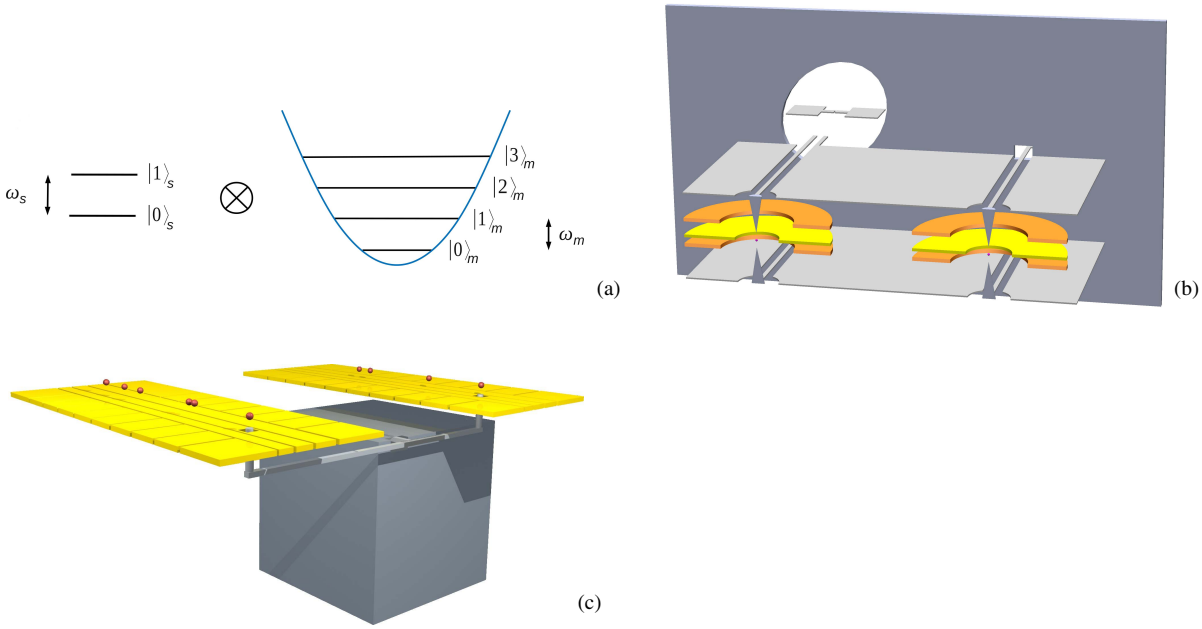

Figure 5. Single electron qubit, and devices using the toolbox developed here. (a) Our scheme uses the electron spin as a quantum memory, and one mode of its harmonic motion in the trap as a bus for coupling to electrical circuits. A static magnetic field provides a splitting ω_s of the electron spin manifold, defining the two-level system used to store quantum information. Under a magnetic field of 10^{-3} T, the electron Zeeman splitting is $\omega_s = 2\pi \times 28$ MHz. Typical electron frequencies for the applications we describe will be approximately $\omega_x = \omega_z = 2\pi \times 400$ MHz, $\omega_y = 2\pi \times 500$ MHz. (b) Schematic of an electron–transmon hybrid. Transmons operating inside 3D cavities are the processing qubits, and each one is coupled to an electron quantum memory via a $\lambda/2$ resonator. (c) Schematic of an all-electron architecture. Electrons are trapped on a segmented Paul trap. They can be shuttled to regions where their motion is parametrically coupled to microwave resonators and to transmon qubits (inside gray box). Electron–electron gates can be performed via direct Coulomb interaction for electrons on the same trap chip, and using a microwave bus for electrons on different chips. In (b) and (c), the electron traps can be operated at a different temperature stage (e.g. 1 K, yellow and orange) from the superconducting electronics (30 mK, gray) to minimize the heat load on the latter.

superconducting circuits, see figure 5. One possibility is for the transmon qubits to function as processing units, and the electron spins to serve as a quantum memory (figure 5(b)). A second possibility is to use the trapped electrons as both processing and memory units, with a CPW bus to perform state transfer and entangling gates between distant electrons, and the transmon serving as a state readout device. A third option uses moving electron qubits in segmented linear Paul traps, much the same way in which ion-trap based scalable QIP is pursued, and transmon qubits for the electron state readout (figure 5(c)) [25, 39].

The first two types of architecture can be implemented using the building blocks shown in figure 5(b). In both cases, the *LC* resonator-based ground state cooling of the electron,

and the magnetic-field based spin–motion coupling serve to initialize the electron state. If the superconducting qubits are used as computational qubits, the SWAP operation between electron and transmon allows information exchange between the processing and memory qubits. In the case of electron-based QIP, SWAP operations allow transfer of information between different electrons. Single qubit rotations can be performed on the electron spin, which together with the $\sqrt{\text{SWAP}}$ gates between the motion of different electrons offer a universal set of gates. One way to read out the state of the electron is by coupling the electron motion to a dressed 3D transmon, as described above, but alternative architectures would be sufficient for this task.

Our proposed parametric frequency conversion mechanism can be applied to linear microfabricated Paul traps for electrons. In this case, ground state cooling of the electron motion, state initialization and readout of the electron spins can be based on microwave circuits. This enables a third distinct architecture, which uses moving electron qubits, similar what is currently pursued with trapped ions [39]. Two-qubit entangling gates can be performed using a microwave bus, the direct Coulomb interaction between nearby electrons [5], or with microwave gates [36]. Finally, nonlinear superconducting circuits can be used to read out the state of the electrons. This approach will not require lasers for cooling, manipulating and detecting the electron qubits, as trapped-ion based approaches do. In addition, it can be significantly faster than current ion-trap based approaches. State initialization and read-out can be performed on the order of a few μs, roughly two orders of magnitude faster than with ions. Owing to the higher electron frequencies, particle transport can also be two orders of magnitude faster. Two-electron gates based on the Coulomb interaction of nearby electrons, will be limited by the rate of spin–motion coupling that can be achieved. This can be more than one order of magnitude faster than the values achieved with ions, due to the larger extent of the electron's wavefunction in the ground state.

As a final, longer-term application, we consider scaling an architecture similar to that of figure 5(c) to sub-micrometer dimensions, and operating it *entirely* on a 1 K refrigeration stage. This would allow fast gate operation times and overcome the problem of limited cooling power of dilution refrigerators, typically in the sub-mW range. Miniaturized linear Paul traps for electrons, with typical electron–electrode distances of 500 nm could achieve secular frequencies of $2\pi \times 20$ GHz and depths of 10 meV, with moderate trapping voltages of less than 1 V. The parametric upconversion mechanism, described in section 2, applied to this case would allow coupling to superconducting resonators with frequencies above $2\pi \times 100$ GHz [40, 41] enabling ground-state cooling of the electrons in $\sim$4 ns, using a 1 K thermal bath. Electron transport, swapping and entangling gates could be performed in time of order 0.1 ns. To read out the electron motional state, mapping to a superconducting qubit, as outlined above, is one option, but an alternative option would be dispersive circuit quantum electrodynamics (CQED) type read-out [34] on the $\{|0\rangle, |1\rangle\}$ manifold of the electron motion.

A number of technical challenges would need to be overcome in such an approach. Device miniaturization will not be feasible before the electrode surface noise sources are eliminated at cryogenic temperatures, for example reduction by three orders of magnitude over current values would imply electron heating rates of order 3×10^4 quanta s^{-1} in the example mentioned here. In addition, the technology of millimeter wave sources and resonators in the millimeter frequency band, above $2\pi \times 100$ GHz, would need to be adapted to the high-fidelity, low-loss demands of QIP applications.

6. Conclusion

In summary, we have proposed a parametric frequency conversion scheme which can bridge the frequency gap between the motion of trapped particles in Paul traps and solid-state quantum circuits operating in the microwave regime. Our scheme uses geometric nonlinearities of the trap electrodes, and can be implemented in standard trap geometries without the need for actively driven, solid-state frequency conversion devices. In addition, it up-converts the trapped particle signal before this enters the solid state, and can thus reduce the impact of $1/f$ noise. This scheme allows to implement swapping and entangling operations between electrons and superconducting electronics, and can be used to initialize and read-out the state of an electron, as well as to use the electron spin as a quantum memory for superconducting qubits. Using currently achievable parameters for the device components, we find that all basic operations necessary for QIP can be carried out with fidelities close to 99%. We have described applications of this scheme to hybrid quantum architectures in which both trapped electron spins and transmon circuits serve as processing qubits. Our toolbox enables a QIP architecture with electrons, similar to the one currently pursued with trapped ions in segmented traps, but having advantages in speed and scalability.

Acknowledgments

We acknowledge useful discussions with I Siddiqi, K Murch and with P K Day. This research was funded by the Office of the Director of National Intelligence (ODNI), Intelligence Advanced Research Projects Activity (IARPA), through the Army Research Office grant W911NF-10-1-0284, by AFOSR through the ARO grant FA9550-11-1-0318, by NSF under NSF-DMR-0956064, NSF-CCF-0916303 and by Agilent under ACT-UR 2827. All statements of fact, opinion or conclusions contained herein are those of the authors and should not be construed as representing the official views or policies of IARPA, AFOSR, the ODNI, or the US Government.

Appendix A. Capacitive coupling of classical signals to the quantum bus

In the geometries outlined in figures 2 and 3, the classical drive used to trap the electrons and to pump the parametric action can couple to the CPW used as a quantum bus, and cause off-resonant excitations. Conversely, if the CPW couples to the transmission lines used to drive the trap and the parametric action, then it will radiatively decay into the transmission lines. To minimize these effects, one needs to capacitively drive opposite ends of the $\lambda/2$ CPW resonator (figure 3(b)) in such a way that the most of the capacitive coupling cancels out, or use some equivalent scheme. Capacitive coupling of the CPW to a 50 Ω feed line or *LC* resonator used to drive the trap electrodes will only limit the quality factor at the 10^7 level if the coupling capacitance is limited to below 0.2 fF. Here we describe a scheme which is mainly aimed at cancelation of the off-resonant excitation, while achieving far greater reduction of the radiative losses.

To minimize off-resonant excitations, we need to carefully balance capacitances in the device and weakly couple in an additional 'fine-tuning' signal. One possible solution is outlined in figure A.1. The signal, which is capacitively coupled via a parasitic capacitance C_p, to the coupling electrode, is also coupled with an appropriate amplitude to the opposite end of the $\lambda/2$

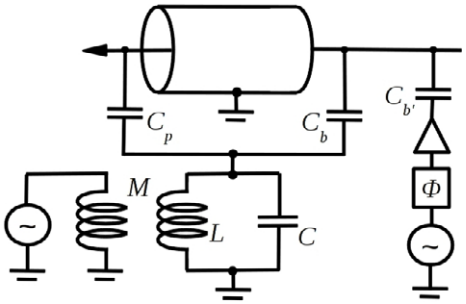

Figure A.1. Circuit to minimize classical pick-up on the CPW quantum bus, and radiative decay of the bus. For simplicity, the ring electrodes (trapping and parametric drive electrodes) are designated by the parasitic capacitances which they contribute. The signal which is capacitively coupled via C_p to the coupling electrode, is also coupled with an appropriate amplitude to the opposite end of the $\lambda/2$ resonator, via the balancing capacitance C_b. An additional 50 Ω line is directly coupled to one end of the CPW bus via a small coupling capacitance $C_{\mathrm{b}'}$.

resonator, via the balancing capacitance $C_\mathrm{b} \approx C_\mathrm{p}$. Both capacitors are connected to a resonator with characteristic impedance $Z = \sqrt{L/C} \approx 50\,\Omega$, and moderate quality factor $Q \approx 10^3$, which is used to drive the trap electrodes, and helps minimize radiative losses of the $\lambda/2$ resonator. An additional 50 Ω transmission line is capacitively coupled with $C_{\mathrm{b}'} \ll C_\mathrm{p}$ to one end of the $\lambda/2$ resonator, and driven with an adjustable amplitude and phase shift, in order to fine-tune the cancelation of the off-resonant excitation. The parasitic capacitances in the ring trap described here are on the order of 0.5 fF, and if they are balanced to $C_\mathrm{p} - C_\mathrm{b} \approx 10$ aF, the off-resonant excitation of the $\lambda/2$ resonator will amount to approximately 200 photons. To fine-tune the cancelation to the level of 10^{-3} photons, the amplitude and phase in an additional 50 Ω line, coupled by $C_{\mathrm{b}'} \approx 10$ aF needs to be adjusted at the 0.4 mV level, provided the phase is controlled to better than $\phi = 10^\circ$.

This configuration also minimizes the inverse effect of radiating from the CPW into the classical-signal transmission lines. Due to the use of an LC resonator which is far detuned from the CPW bus and of a weakly coupled transmission line, the radiative loss of the CPW to the external lines will be limited to the level of $\kappa < 1/\mathrm{s}$.

Appendix B. Decoherence of the electron motion

To estimate the heating rate of the electron motion in the y-direction, we need to know the spectral density of electric field noise at $\omega_y \approx 2\pi \times 500$ MHz [15]. Johnson noise and electronic technical noise can be made very small, so we focus on the so called 'anomalous' heating, encountered in ion traps. The dominant contribution of this noise has been shown to arise from the electrode surfaces [42]. We can model the noise as arising from a collection of independently fluctuating electrical-dipole type sources on the trap electrodes, in which case the noise level is determined by the surface density of electrical dipoles on the electrodes [43, 44]. In this model, the magnitude of the noise for a given density of dipoles has been shown to depend on the electrode geometry [45]. We take into account the non-planar geometry of the proposed trap by incoherently summing the contributions of all dipoles on the surface of the electrodes. For each

one of the conical tips with opening angle α, we find that the noise is reduced over the noise generated by a flat surface. For low opening angles the noise level at distance R_0 from the tip is well approximated by

$$S_{\mathrm{E}}^{\mathrm{tip}}(R_0, \alpha) \approx (\alpha/10) S_{\mathrm{E}}(R_0, \pi), \tag{B.1}$$

where $S_{\mathrm{E}}(R_0, \pi)$ is the noise at a distance R_0 from a flat surface (i.e. a cone of opening angle π). Similarly, for a ring electrode similar to the one in figure 1, the noise contribution is estimated at

$$S_{\mathrm{E}}^{\mathrm{ring}}(D, a) \approx 2\left(1 + \frac{2a}{D}\right) S_{\mathrm{E}}(D/2, \pi), \tag{B.2}$$

i.e. each one of the top and bottom surfaces of the ring contributes the same noise as a flat plane located a distance $D/2$ from the ion ($S_{\mathrm{E}}(D/2, \pi)$), and the inside surface of the ring contributes a fraction $2a/D$ of that noise. The two rings which are used to drive the electron motion (orange in figure 2) can easily be placed a factor of 2 or more further away from the ion compared to the trapping ring electrode, and their contribution can thus be neglected. Taking these results into account, and based on the noise value measured in cryogenic traps [24], the heating rate for an electron trapped at $2\pi \times 500$ MHz in the ring trap discussed here, is estimated at 8100 motional quanta/s if the frequency scaling of the noise is $1/f$, and at 690 quanta s^{-1} if the scaling is $1/f^{3/2}$.

Appendix C. Parametric drive of the electron motion

As discussed in the main text, the parametric coupling can be switched on by driving classical electron motion. Electron motion can be driven in the y-direction, but also in the x-direction. To achieve the latter, we can split the trapping ring electrode into two half rings on the sides of the yz plane, and apply a classical out-of-phase drive to the two sides. This option comes at the expense of a factor of 2 reduction in the parametric coupling rate and here we focus on driving the y motion. The trap drive and the parametric drive of the electron motion are detuned from the superconducting electronics by $\approx 2\pi \times 500$ MHz. In order to drive electron motion in the y-direction at $\Omega_{\mathrm{d}} \approx 2\pi \times 6.5$ GHz and $A_{\mathrm{d}} = 750$ nm, we apply an oscillating voltage of amplitude 0.4 V on the ring electrodes labeled $\pm V_{\mathrm{d}}$ in figure C.1 below. Numerical integration of the electron equations of motion, with both the trapping potential at Ω_{tr} and the drive at Ω_{d}, shows that the trap is stable, and motional sidebands appear at frequencies $\Omega_{\mathrm{d}} + n\Omega_{\mathrm{tr}} \pm \omega_i$, $n = 0, \pm 1, \ldots$. If $\Omega_{\mathrm{tr}} = \Omega_{\mathrm{d}}$ only sidebands at $\Omega_{\mathrm{d}} \pm \omega_i$ are present, and this can be a preferable configuration.

It is interesting to consider the limits of applying the proposed parametric scheme to trapped ions, by analyzing the influence on the trapping pseudopotential when $\Omega_{\mathrm{tr}} = \Omega_{\mathrm{d}}$. The parametric pump field generates a pseudopotential which is not significant for electrons under the trapping conditions we described above. The situation is different for ions, because of their lower secular frequencies. To see this, we compare two energy scales: The strength of the pseudopotential, $U_{\mathrm{ps,d}}$, which arises from the parametric drive when the driven motion amplitude is A_{d}, and the trapping potential with curvature $\frac{1}{2}m\omega^2$. The ratio of the two is $\frac{U_{\mathrm{ps,d}}}{m\omega^2 A_{\mathrm{d}}^2} \approx \frac{1}{4}\left(\frac{\Omega_{\mathrm{d}}}{\omega}\right)^2$. So the pseudopotential arising from the parametric drive scales quadratically with the driven motion amplitude, and with the frequency step-up. For example, for $^9\mathrm{Be}^+$ with secular frequency of 2 MHz in a trap such as the one described here, the limiting frequency is

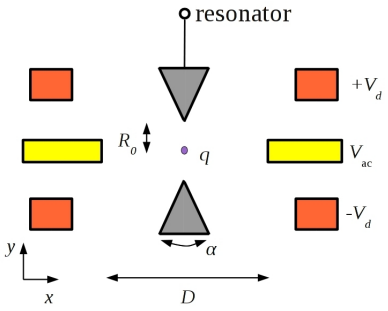

Figure C.1. Cross section of the trap, with the different electrodes labeled. We use the parameters $D = 30\,\mu$m, $R_0 = 5\,\mu$m, opening angle $\alpha = 20^\circ$. In order to drive electron motion in the y-direction at $\Omega_d \approx 2\pi \times 6.5$ GHz and $A_d = 750$ nm, we apply to the top and bottom drive electrodes (orange) an oscillating drive with opposite amplitudes $\pm V_d \cos(\Omega_d t)$, where $V_d = 0.4$ V.

approximately $2\pi \times 2$ GHz. For higher frequencies it becomes hard to control nonlinearities in the trap potential.

We note here that the mechanism described in section 2 applies to a particle in a harmonic trap with coupling electrodes which produce a quadrupole potential. This mechanism does not rely on the existence on the so-called 'micromotion sidebands', which in a Paul trap appear at frequencies $n\,\Omega_{tr} \pm \omega_i$, $n = 1, 2, \ldots$, $i = x, y, z$. With our choice of parametric drive frequency and coupling electrode (which creates a quadrupole potential), the micromotion sidebands do not couple the particle and the circuit. Under a geometry in which the coupling electrodes produce a dipole-type potential (e.g. parallel-plate capacitor type coupling electrodes), the micromotion sidebands can couple the particle motion to a circuit at $\Omega_{tr} \pm \omega_i$. This type of frequency-conversion mechanism will have limited effectiveness for high frequency step-up (large $(\Omega_{tr} \pm \omega_i)/\omega_i$), and its treatment is beyond the scope of this work.

Appendix D. Decoherence of the coplanar waveguide resonator

The internal quality factor (Q_i) of CPW resonators is thought to be limited by fluctuating two-level systems in the interface between the superconductor and the dielectric substrate on which it is fabricated [46–48]. As a result, Q_i decreases by one–two orders of magnitude as the energy stored in the resonator decreases to the few photon level. In recent years, significant efforts in dielectric substrate cleaning and materials engineering have resulted in an increase of Q_i [49, 50], with values at the single photon level currently exceeding 10^6 [30]. Moreover, it has been realized that the resonator losses can be limited by reducing the participation of the dielectric-superconductor interface in the resonant mode. One way to achieve this is by building higher characteristic impedance CPW resonators [51]. This can prove advantageous for the high characteristic impedance resonators $Z_{CPW} \sim 1\,$kΩ needed in our application. TiN-based high kinetic inductance resonators in the $2\pi \times 1$–2 GHz range, already mentioned in section 3, show very high quality factors [31], and due to their high kinetic inductance have wavelength significantly lower than the vacuum wavelength, which significantly reduces their radiative losses. In this work, we assume a resonator with quality factor similar to the best value obtained by Megrant *et al* [30], with $\tau_1 = 45\,\mu$s at $\approx 2\pi \times 7$ GHz.

Appendix E. Electrical resonator and cavity interaction

In order to couple the CPW transmission line to the transmon cavity, perhaps the simplest option is for the center conductor and one side of the ground plane of the line to extend into the cavity, with an appropriate modification in geometry to maintain the impedance of the transmission line constant. To estimate the interaction strength of the transverse electromagnetic (TEM) mode of the CPW to the TE_{011} mode of the cavity, we treat the transmission line as a collection of electrical dipoles formed between the center conductor and ground. The dipoles arise from the local charge density on the CPW and they form a continuous distribution over its length. A segment of length dz along the line direction (z) has dipole strength $\mu(z) \approx \frac{2\pi d_0 q_0}{\lambda} \sin(2\pi z/\lambda)$. Here d_0 is the spacing between the CPW center and signal return conductors $q_0 = \sqrt{\frac{\hbar}{2Z}}$ is the magnitude of charge fluctuations in the line, and λ is the wavelength of the wave in the CPW. If the electric field of the TE_{011} cavity mode, $E_C(z)$, is aligned with the dipoles (i.e. if it is along the line connecting the center conductor to ground), then an upper limit for the coupling strength can be expressed as the integral $\hbar G_{lc} = \frac{1}{l}\int_0^l \mu(z)\, E_C(z)\, dz = \frac{E_{C,0} q_0 d_0\, l_{eff}}{\lambda}$, where $E_{C,0} = \sqrt{\frac{\hbar\omega_C}{2\epsilon_0 V}}$ is the magnitude of electric field fluctuation in the cavity, and the effective length l_{eff} can be up to order $\lambda/2$.

We consider a cavity at $2\pi \times 7$ GHz, and a CPW with effective impedance of 1 kΩ. A lower limit for d_0 is 200 μm, which implies that $G_{lc}/\hbar$ can be $2\pi \times 10$ MHz, for $l_{eff} = \lambda/2$. Our architecture requires lower values, in the 3 MHz range, which can be achieved with appropriate design.

Appendix F. Electron–transmon quantum electrodynamics

The electron–transmon system is at heart a problem of four coupled quantum systems: three oscillators and a qubit. The electron motion, intermediate quarter wave resonator, and transmon cavity function as harmonic oscillators, while the transmon acts as a qubit. It is illustrative to write the effective four-system problem by an effective Hamiltonian

$$H_{\text{eff}} = \mathbf{a}^\dagger \begin{pmatrix} \omega & g_p & 0 & 0 \\ g_p & \omega+\delta & G_{lc} & 0 \\ 0 & G_{lc} & \omega+\Delta & G_{tc} \\ 0 & 0 & G_{tc} & \omega' \end{pmatrix} \mathbf{a} = \mathbf{a}^\dagger \mathbf{C} \mathbf{a} \tag{F.1}$$

with $\mathbf{a} = (a_x, a_\phi, a_c, \sigma_-)^T$, the vector of excitation annihilation operators for the electron, transmission line, transmon cavity and transmon respectively. For presentation, we have absorbed all the time-dependent factors into the definitions of $\mathbf{a}$ and $\mathbf{a}^\dagger$. Such a formulation is useful because the coupling matrix $\mathbf{C}$ contains the relevant dynamics. The excitation energies are read off from the diagonal elements, and the coupling rates are read off from the off-diagonal elements.

In the limit where the cavity–transmon coupling is the strongest ($G_{tc} \gg G_{lc}, g_p$), we can view the eigenstates of the cavity–transmon system as the modes of interest, and focus on coupling to the transmon dressed state. Then, the problem can be reduced to an effective three-system problem in the following way. First, we diagonalize the cavity–transmon block in the limit $\Delta \gg G_{tc}$. After the diagonalization we get two vectors: one with a projection mostly onto the transmon mode (which we referred to as the 'dressed transmon'), and with a projection onto

the cavity mode only of order G_{tc}/Δ. The second has a projection mostly onto the cavity mode and projects onto the transmon mode also to order G_{tc}/Δ.

The first vector represents the operator $\sigma_+ + (G_{tc}/\Delta)a_c^\dagger$. This is a Hamiltonian operator for a dressed transmon mode. The second vector is similar, representing a mode which lives primarily in the cavity. Since we have earlier chosen the cavity to be far detuned from the transmon, this mode can be adiabatically eliminated. Removing this dressed cavity mode from the basis produces a reduced coupling matrix

$$\mathbf{C}_{\text{red}} = \begin{pmatrix} \omega & g_p & 0 \\ g_p & \omega + \delta & -G_{lc}G_{tc}/\Delta \\ 0 & -G_{lc}G_{tc}/\Delta & \omega \end{pmatrix}. \tag{F.2}$$

By adjusting G_{lc} and Δ so that $G_{lt} = G_{lc}G_{tc}/\Delta = g_p$, we can obtain complete state transfer and entanglement between the electron motion and the dressed transmon, as we discuss in the main text.

References

[1] DiVincenzo D P 2000 *Fortschr. Phys.* **48** 771–83
[2] Ladd T D *et al* 2010 *Nature* **464** 45–53
[3] Häffner H *et al* 2008 *Phys. Rep.* **469** 155
[4] Sørensen A S *et al* 2004 *Phys. Rev. Lett.* **92** 063601
[5] Ciaramicoli G *et al* 2003 *Phys. Rev. Lett.* **91** 017901
[6] Tian L *et al* 2004 *Phys. Rev. Lett.* **92** 247902
[7] Daniilidis N and Häffner H 2012 *Annu. Rev. Condens. Matter Phys.* **4** 83–112
[8] Heinzen D J and Wineland D J 1990 *Phys. Rev.* A **42** 2977
[9] Kielpinski D *et al* 2012 *Phys. Rev. Lett.* **108** 130504
[10] Wineland D J and Dehmelt H G 1975 *J. Appl. Phys.* **46** 919
[11] Schuster D I *et al* 2010 *Phys. Rev. Lett.* **105** 040503
[12] Walz J *et al* 1995 *Phys. Rev. Lett.* **75** 3257–60
[13] Hoffrogge J *et al* 2011 *Phys. Rev. Lett.* **106** 193001
[14] Wineland D J *et al* 1998 *J. Res. Natl Inst. Stand. Technol.* **103** 259–328
[15] Deslauriers L *et al* 2006 *Phys. Rev. Lett.* **97** 103007
[16] Bushev P *et al* 2011 *Eur. Phys. J.* D **63** 9–16
[17] Louisell W *et al* 1961 *Phys. Rev.* **124** 1646
[18] Braunstein S L and Loock P V 2005 *Rev. Mod. Phys.* **77** 513–77
[19] Mishkin E A and Walls D F 1969 *Phys. Rev.* **185** 1618
[20] Paik H *et al* 2011 *Phys. Rev. Lett.* **107** 240501
[21] Rigetti C *et al* 2012 *Phys. Rev.* B **86** 100506
[22] Koch J *et al* 2007 *Phys. Rev.* A **76** 042319
[23] Singer K *et al* 2010 arXiv:0912.0916
[24] Brown K R *et al* 2011 *Nature* **471** 196–9
[25] Kielpinski D *et al* 2002 *Nature* **417** 709–11
[26] Amini J M *et al* 2010 *New J. Phys.* **12** 033031
[27] Wineland D J *et al* 1973 *Phys. Rev. Lett.* **31** 1279–82
[28] Karin T *et al* 2011 *Appl. Phys.* B **106** 117
[29] Kumph M *et al* 2011 *New J. Phys.* **13** 073043
[30] Megrant A *et al* 2012 *Appl. Phys. Lett.* **100** 113510
[31] Leduc H G *et al* 2010 *Appl. Phys. Lett.* **97** 102509

[32] Zmuidzinas J 2012 *Annu. Rev. Condens. Matter Phys.* **3** 169–214
[33] Day P K 2013 private communication
[34] Blais A *et al* 2004 *Phys. Rev.* A **69** 062320
[35] Sørensen A S and Mølmer K 2000 *Phys. Rev.* A **62** 022311
[36] Ospelkaus C *et al* 2008 *Phys. Rev. Lett.* **101** 90502
[37] Ospelkaus C *et al* 2011 *Nature* **476** 181–4
[38] Robbes D 2006 *Sensors Actuators* A **129** 86–93
[39] Hanneke D *et al* 2009 *Nature Phys.* **6** 13–6
[40] Goy P *et al* 1983 *Phys. Rev. Lett.* **50** 1903
[41] Zmuidzinas J *et al* 1994 *IEEE Trans. Microw. Theory Tech.* **42** 698
[42] Hite D A *et al* 2012 *Phys. Rev. Lett.* **109** 103001
[43] Daniilidis N *et al* 2011 *New J. Phys.* **13** 013032
[44] Safavi-Naini A *et al* 2011 *Phys. Rev.* A **84** 023412
[45] Low G H *et al* 2011 *Phys. Rev.* A **84** 053425
[46] Gao J *et al* 2007 *Appl. Phys. Lett.* **90** 102507
[47] Gao J *et al* 2008 *Appl. Phys. Lett.* **92** 152505
[48] Kumar S *et al* 2008 *Appl. Phys. Lett.* **92** 123503
[49] Wang H *et al* 2009 *Appl. Phys. Lett.* **95** 233508
[50] Vissers M R *et al* 2010 *Appl. Phys. Lett.* **97** 232509
[51] Geerlings K *et al* 2012 *Appl. Phys. Lett.* **100** 192601